

Engineering Deep Representations for Modeling Aesthetic Perception

Yanxiang Chen, Yuxing Hu, Luming Zhang, Ping Li, and Chao Zhang

Abstract—Many aesthetic models in multimedia and computer vision suffer from two shortcomings: 1) the low descriptiveness and interpretability¹ of the hand-crafted aesthetic criteria (*i.e.*, fail to indicate region-level aesthetics), and 2) the difficulty of engineering aesthetic features adaptively and automatically toward different image sets. To remedy these problems, we develop a deep architecture to learn aesthetically-relevant visual attributes from Flickr², which are localized by multiple textual attributes in a weakly-supervised setting. More specifically, using a bag-of-words (BoW) representation of the frequent Flickr image tags, a sparsity-constrained subspace algorithm discovers a compact set of textual attributes (*i.e.*, each textual attribute is a sparse and linear representation of those frequent image tags) for each Flickr image. Then, a weakly-supervised learning algorithm projects the textual attributes at image-level to the highly-responsive image patches. These patches indicate where humans look at appealing regions with respect to each textual attribute, which are employed to learn the visual attributes. Psychological and anatomical studies have demonstrated that humans perceive visual concepts in a hierarchical way. Therefore, we normalize these patches and further feed them into a five-layer convolutional neural network (CNN) to mimic the hierarchy of human perceiving the visual attributes. We apply the learned deep features onto applications like image retargeting, aesthetics ranking, and retrieval. Both subjective and objective experimental results thoroughly demonstrate the superiority of our approach.

Index Terms—Machine learning, Deep architecture, Flickr,

Copyright (c) 2010 IEEE. Personal use of this material is permitted. However, permission to use this material for any other purposes must be obtained from the IEEE by sending a request to pubs-permissions@ieee.org. (Y. Hu is the correspondence author of this article.) This work is in part supported by the National Basic Research Program under grant 2013CB336500, by the National High-Tech Development Program under grant 2014AA015104, by the Fundamental Research Funds for the Central Universities, by the Program for New Century Excellent Talents under grant NCET-130764, the Project from National Nature Science Foundation of China under grant 61472116, 61572169, 61672201, the Anhui Fund for Distinguished Young Scholars grant 1508085J04, and the National University of Singapore (Suzhou) Research Institute, 377 Lin Quan Street, Suzhou Industrial Park, Jiang Su, Peoples Republic of China, 215123. Ping Li’s work was supported in part by the National Natural Science Foundation of China under Grant 61502131, Zhejiang Provincial Natural Science Foundation of China under Grant LY18F020015 and LQ15F020012.

Y. Chen and L. Zhang are with the Department of CSIE, Hefei University of Technology, Hefei, China.

Y. Hu is with the School of Aerospace Engineering, Tsinghua University, Beijing, China.

P. Li is with the School of Computer Science and Technology, Hangzhou Dianzi University, Hangzhou 310018, China, and also with State Key Laboratory for Novel Software Technology, Nanjing University, Nanjing 210093, China (e-mail: patriclouis.lee@gmail.com).

C. Zhang is with the Department of Computer Science University of Illinois at Urbana-Champaign, USA.

Attributes, Convolutional neural network

I. Introduction

Perceptually aesthetic modeling refers to the process of discovering low-level and high-level visual patterns that can arouse human aesthetic perception. It is a useful technique to enhance many applications, *i.e.*, image retargeting, photo album management, and scene rendering. Taking retargeting as an example, the aesthetically pleasing image regions are squeezed slightly and vice versa. Moreover, effectively describing region-level aesthetics can guide the level of details in non-photorealistic image rendering. As a popular media sharing website with millions of photos uploaded and commented daily, Flickr is an ideal platform to study and simulate how humans perceive photos with aesthetic features at low&high-level. However, perceptually aesthetic modeling based on Flickr still encounters the following challenges:

- Flickr contains a large amount of photos with multiple latent aesthetic attributes (*e.g.*, the “field guide” and “movement”). Conventional aesthetic models, however, are typically built upon generic features which quantify the compliance to a pre-defined criterion (*e.g.*, the “rule of thirds”). Practically we need tailored and datasetdependent features to capture these latent aesthetic attributes, but engineering these features requires the domain knowledge of professional photographers.
- The interpretability of an aesthetic model reflects the capability of indicating which regions are responsive to each aesthetic attribute. A highly interpretable aesthetic model has both the scientific impact and application value. As far as we know, however, the existing aesthetic modeling pipeline is more or less a blackbox. They have limited power to provide region-level response to each aesthetic attribute. In this work, textual attribute means a combination of those frequent image tags, such as “portrait”, “beach”, and “art”, which are discovered automatically.
- Previous methods associate each photo with a set of aesthetic attributes only in well-controlled settings. For example, the training images’ beautifulness is quantified to reduce the disturbance of noisy tags [2]. In reality, image tags from Flickr are labeled uncontrollably by a rich variety of users with diverse backgrounds, education, *etc.* This will inevitably produces noisy image tags, which necessitates an aesthetic model to robustly tackle noises from image tags.

To solve these problems, we propose a CNN-based framework which models aesthetic perception automatically and interpretably, by calculating a compact set of textual and visual attributes from tagged Flickr images. The pipeline of our proposed framework is elaborated in Fig. 1. For each tagged image from an Internet-scale Flickr corpus, we employ a bag-of-words (BoW) representation of those frequently-occurring and

¹ In this work, “describing” and “interpretability” means the ability of seeking region-level representation of each mined textual attribute, *i.e.*, a

sparse and linear representation of those frequent image tags.

²<https://www.flickr.com/>

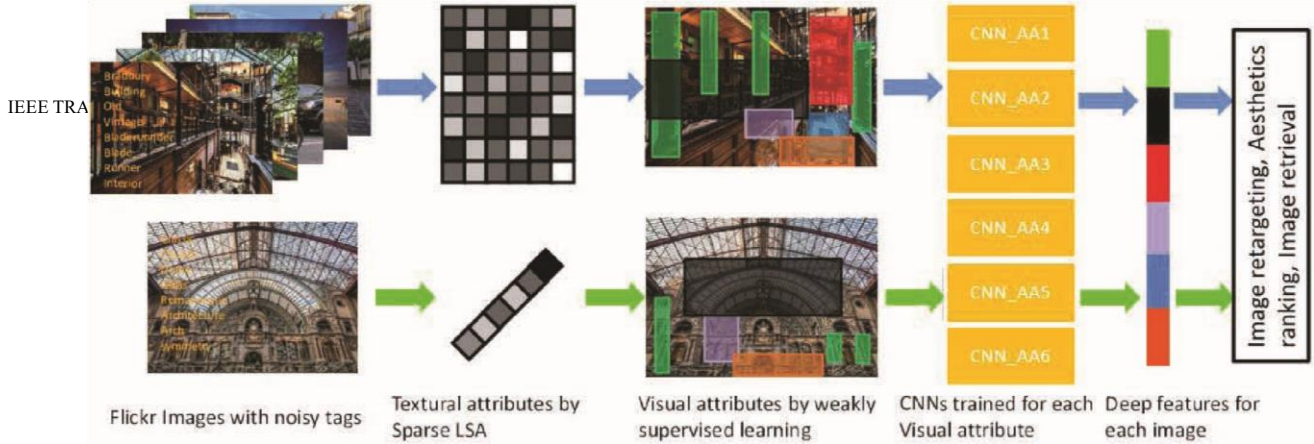


Fig. 1. The pipeline of the proposed CNN-based aesthetic modeling framework (The blue and green arrows denote the training and test phases respectively. The color-tagged regions indicate visual attributes which are aesthetically pleasing. CNN AA i means the sub-network trained from the i -th visual attribute.).

noisy image tags. Toward an efficient system, a sparsity-constrained subspace algorithm converts each BoW histogram into a compact set of textual attributes. They reflect the highly representative aesthetic attributes of an image. To locate the appealing visual attributes, a weakly supervised algorithm maps the textual attributes at image-level into the salient patches (indicated by different colors in the middle of Fig. 1) in an image. Both psychological and anatomical studies have shown that human vision system is multi-layered and forms higher-level abstracts from input raw pixels incrementally. That is to say, the intrinsic hierarchy of CNN has the potential to model human visual perception. Based on this, for each textual attribute, the corresponding extracted patches are employed to learn a five-layer CNN to simulate the hierarchical perception of human beings. The learned deep feature is applied on a range of multimedia tasks: image retargeting, aesthetics classification, and image retrieval.

The contributions of this paper can be summarized as: 1) The first deep architecture that learns aesthetically-relevant visual attributes extracted from massive-scale Flickr images; 2) a weakly supervised algorithm associating each textual attribute with the corresponding visual attribute; and 3) adopting the deep features on several multimedia applications, coupled with extensive experimental validation.

II. Related Work

Our work is related to two research topics in multimedia and pattern recognition: computational image aesthetics analysis and deep learning for aesthetic attribute modeling.

A. Computational Image Aesthetic Analysis

1) *Global features-based models:* Datta *et al.* [3] proposed 58 low-level visual features, *e.g.*, the shape convexity, to capture photo aesthetics. Dhar *et al.* [5] proposed a set of high-level attribute-based predictors to evaluate photo aesthetics. In [6], Luo *et al.* employed a GMM-based hue distribution and a prominent line-based texture distribution to assess the global composition of an image. To represent image local composition, regional features describing human faces, region clarity, and complexity were developed. In [7], Marchesotti *et al.* tackled the problem of visual aesthetic modeling by discovering mid-level features. The designed algorithm can automatically learn semantic aesthetics-related attributes by combining image, scoring, and textual data from the AVA data set [2]. The authors shown that the learned attributes can facilitate a variety of media applications, *e.g.*, aesthetic quality prediction, image

tagging, and retrieval. Experiments shown that the above two generic descriptors outperform many hand-crafted and dataset-dependent aesthetic descriptors.

2) *Local feature-based models:* Cheng *et al.* [36] proposed the omni-range context, *i.e.*, the spatial distribution of arbitrary pairwise image patches, to describe image composition. Nishiyama [9] *et al.* first detected multiple subject regions inside a photo. Afterward an SVM classifier is trained for each subject region. Finally, the aesthetics of an image is quantified by combining the SVM scores of a photo's internal subject regions. In [10], Nishiyama *et al.* proposed a color harmony-based aesthetic model, which describes image color distribution using its patches. The patch-level color distribution is integrated into a BoW histogram, which is subsequently classified by an SVM to determine whether a photo is highly or low aesthetic. Bhattacharya *et al.* [11] developed a spatial recombination system which allows users to select a foreground object interactively. The system presents recommendations to indicate an optimal location of the foreground object, which is detected by combining multiple visual features.

B. Deep learning-based Aesthetics Modeling

As far as we know, there are only two deep learning models for visual aesthetic analysis. In [22], Lu *et al.* proposed a double-layer CNN architecture to automatically discover effective features that capture image aesthetics from two heterogeneous input sources, *i.e.*, aesthetic features from both the global and local views. The double CNN layers are jointly trained from two inputs. The first layer takes global image representation as the input, while the second layer takes local image representations as the input. This allows us to leverage both compositional and local visual information. Based on the evaluation from the AVA [2], Lu *et al.*'s algorithm significantly outperforms the results reported earlier. This model differs from ours fundamentally in two aspects: 1) Both the global and local views are heuristically defined, there is no guarantee that they can well locate the aesthetically pleasing regions across different datasets. Comparatively, our approach uses a weakly supervised algorithm to discover visually appealing regions indicated by tags. Thus it can be flexibly adapted onto different datasets; 2) Lu *et al.*'s model simply captures the global and local aesthetic features of a photo. But there is no evidence that abstract aesthetic cues can be well described. Noticeably, in our model, a set of CNNs are trained. Each encodes the visual attribute corresponding to a textual attribute, which can capture

either a concrete or abstract aesthetic cue. In [23], Champbell *et al.* trained two Restricted Boltzmann Machines (RBMs) on the highly and low aesthetic images respectively. The authors observed that 10% of the filters learned from the highly aesthetic images capture the aesthetics-relevant visual cues. But this model is only available on simple abstract paintings with low resolution. It is intractable to describe high resolution Flickr images with sophisticated semantics. Escorcía *et al.* [55] established a deep architecture to learn visual semantic attribute. Empirical results shown that the attribute centric nodes in the conv-net encodes information that precisely reconstructs attributes in a sparse and unevenly distributed way.

III. The Proposed Method

A. Sparse Textual Attributes Discovery

Given a Flickr image, we use an M -dimensional augmented frequency vector $\rightarrow\alpha$ to represent the distribution of its tags³. In particular, to avoid the randomly-occurring noisy image tags, we select the M most frequent tags from the training image set. Then, we treat the tag set of each Flickr image as a document D , based on which the i -th element of vector $\rightarrow\alpha$ can be calculated as:

$$\rightarrow\alpha(i) = 0.5 + \frac{f(i, D)}{\max(f(j, D) : j \in D)}, \quad (1)$$

where $f(i, D)$ counts the times of the i -th tag from the M most frequent ones occurring in document d , and the denominator functions as a normalization factor. In our implementation, we set $M = 100$ based on cross validation.

Given N Flickr images, they can be represented as N augmented frequency vectors. Thereafter, we column-wise stack them into a matrix $X = [\rightarrow\alpha_1; \rightarrow\alpha_2; \dots; \rightarrow\alpha_N] \in \mathbb{R}^{N \times M}$, where each row $X_{\cdot j} \in \mathbb{R}^N$ denotes the j -th feature vector cross all the documents. To obtain the textual attributes of each Flickr image, we employ a subspace algorithm, which converts the original M -dimensional vector corresponding to

³In our implementation, we set $M = 100$.

each Flickr image into a D -dimensional textual attribute vector ($D < \min(M, N)$). In our implementation, all the 75246 training images are adopted to create document matrix X .

Following the latent semantic analysis (LSA) [25], we assume that the D textual attributes $\{\vec{u}_1, \vec{u}_2, \dots, \vec{u}_D\}$ are uncorrelated, where each attribute $\vec{u}_d \in \mathbb{R}$ has the unit length, *i.e.*, $\|\vec{u}_d\|_2 = 1$. Denote $U = [\vec{u}_1, \vec{u}_2, \dots, \vec{u}_D] \in \mathbb{R}^{N \times D}$, we have

$U^T U = I$ where I is the identity matrix. We assume that each feature vector $X_{\cdot j}$ can be linearly reconstructed by the textual attributes:

$$X_{\cdot j} = \sum_{d=1}^D a_{dj} \vec{u}_d + \epsilon_j, \quad (2)$$

In the matrix form, the above equation can be reformulated into $X = UA + \epsilon$, where $A = [a_{dj}] \in \mathbb{R}^{D \times M}$ denotes the projection matrix from the tag space to the textual attribute space. We can obtain the projection matrix A by solving the following optimization. It minimizes the rank- D approximation error subject to the orthogonality constraint of U :

$$\min_{U, A} \|X - UA\|_F^2, \quad s.t. \quad U^T U = I, \quad (3)$$

where $\|\cdot\|_F$ denotes the matrix Frobenius norm. The constraint $U^T U = I$ reflects the uncorrelated property of textual attributes.

Sparsity of textual attributes: The projection matrix U learned from (3) can reconstruct matrix X by a linear combination of textual attributes. Typically, the number of textual attributes D is not small². It indicates that aesthetically modeling an Flickr image by analyzing all its correlated textual attributes might be intractable. Toward an efficient approach, we encode a sparsity constraint into (3) in order to achieve a sparse projection matrix A . An entry-wise l_1 -norm of A is added as a regularization term to the loss function. Based on this, we formulate the sparse textual attributes discovery as:

$$\min_{U, A} \|X - UA\|_F^2 + \lambda \|A\|_1, \quad s.t. \quad \|U\|_F = 1, \quad U^T U = I, \quad (4)$$

where $\|A\|_1 = \sum_{d=1}^D \sum_{j=1}^M |a_{dj}|$ is the entry-wise l_1 -norm of A ; and λ is the positive regularization parameter controlling the density of A , *i.e.*, the number of nonzero entries. In general, a larger λ leads to a sparser A . On the other hand, a highly sparse A will lose some relationships between Flickr tags and textual attributes and will in turn harm the reconstruction quality. In practice, it is important to select an appropriate λ to obtain a more sparse A while still maintaining a good reconstruction quality. It is noticeable that (4) is solved by alternatively optimizing matrix U and A , as detailed in [26].

Besides, we can demonstrate that the discovered textual attributes can be represented by the M most frequent tags from the training image set. Based on (2), the tag vector $\alpha_{\cdot j}$ from each Flickr image can be represented by a linear combination of the textual attributes: $X = UA$. Thus it is straightforward to obtain: $U = XA^{-1}$, where matrix U is a $N \times D$ matrix whose columns denote the D textual attributes, matrix $X \in \mathbb{R}^{N \times M}$ represents the N tag vectors from the training data, and $A^{-1} \in \mathbb{R}^{M \times D}$ is the projection matrix. Based on the sparsity constraint in (4), matrix A is sparse and so do A^{-1} . That is to say, each attributes u_i in matrix U can be sparsely represented by a linear combination of the columns of matrix X , where the contribution of the j -th column is indicated by $[A^{-1}]_{ji}$. Here $[\cdot]_{ji}$ indicates the ji -th element of a matrix. In summary, the i th textual attribute can be represented by the non-zero elements in the i -th column of matrix A^{-1} (the dimensionality of each column is M). That is to say, we can name the i -th textual attribute by the frequent tags corresponding to the non-zero elements in the i -th column of matrix A^{-1} .

B. Weakly Supervised Visual Attributes Learning

This section introduces a graphlet-based weakly supervised learning framework to detect visual attributes corresponding to

² As experimented on our own compiled image set, each Flickr image is

associated with 5 textual attributes. In our implementation, the number of textual attributes is set to 14. Towards since there are about 10000 tags in the Flickr image set, the 15 optimal number of

each textual attribute. We first construct a superpixel pyramid which captures objects with different shapes seamlessly. To quantify region-level response to each textual attribute, a manifold embedding algorithm transfers textual attributes into graphlets. Finally, the patch containing graphlets most responsive to each textual attribute form the visual attribute.

Graphlet construction: There are usually millions of raw pixels inside an image, treating each of them independently brings intractable computation. It is generally accepted that pixels within an image are highly correlated with its spatial neighbors. Therefore, we sample a collection of superpixels and use them to construct different objects. As objects with various scales may evoke human aesthetic perception, we construct superpixels with three sizes by overly, moderately, and deficiently segmenting each image. The segmentation is based on the well-known simple linear iterative clustering (SLIC). It is established from the k-means clustering and has a time complexity of $O(N)$, where N is the number of pixels inside an image. Compared with the conventional methods, experiments have shown that SLIC is computationally more efficient, requires less memory, and generates superpixels more adherent to object boundaries. By segmenting each image three times with different SLIC parameters, a superpixel pyramid is constructed to capture objects with different sizes.

As shown in Fig. 2, different objects can be constructed by



Fig. 2. A superpixel pyramid describing the Dubai towers from multiple scales. The first pyramid layer describes the rough outline of the four towers, the surrounding lake and the sky, reflecting textual attributes such as “harmonic” and “symmetric”. The second layer captures the shape of each individual tower, which corresponds to textual attributes such as “flame” and “dynamic”. The third layer encodes the details of the four towers, e.g., the shape tower top. It is highly responsive to textual attributes such as “shape” and “edge”.

a set of spatially neighboring superpixels. More specifically, a graphlet is a moderately sized graph defined as:

$$G = (V, E), \quad (5)$$

where V is a set of vertices, each representing a superpixel; E is a set of edges, each connecting a pair of spatially neighboring superpixels. We call a graphlet t -sized if it is constituted by t superpixels.

Given a t -sized graphlet, we represent it by a $t \times (t+128+9)$ matrix as:

$$M = [M_C, M_T, M_S], \quad (6)$$

where M_C is a $t \times 9$ matrix and each row is the 9-dimensional color moment [29] from a superpixel; M_T is a $t \times 128$ matrix where each row is a 128-dimensional HOG [30] from a superpixel; and M_S is a $t \times t$ adjacency matrix representing the topology of a graphlet. The graphlet extraction is based on random walk on the superpixel mosaic. More specifically, we

first index the superpixels and then select a starting one. Afterward, spatially neighboring superpixels are visited one-by-one until the maximum graphlet size is reached. Due to the number of graphlets is exponentially increasing the maximum graphlet size, we set it to 7 in our work.

Weakly supervised semantic encoding: The textual attributes indicate the aesthetically pleasing regions in a Flickr image. To locate them, we propose a weakly supervised learning algorithm which transfers textual attributes into different graphlets in an image. The objective function is formulated as:

$$\operatorname{argmin}_Y \sum_{ij} \|y_i - y_j\|^2 [l_s(i, j) - l_d(i, j)], \quad s.t., \quad YY^T = I_d, \quad (7)$$

where $Y = [y_1, y_2, \dots, y_n]$, each denoting a d -dimensional post-embedding graphlet from the training images. Y in Eq.(7) is initialized by the vector obtaining by row-wise concatenating matrix M in Eq.(6). The number of graphlets in Y depends on different image sets. In our implementation, the number is 75246. l_s and l_d are functions measuring the semantic similarity and difference between graphlets, which are quantified according to textual attributes. Denoting $\rightarrow n = [n^1, n^2, \dots, n^c]^T$ where n^i is the number of images with the i -th textual attribute, and $c(\cdot)$ contains the textual attributes of the Flickr image from which a graphlet is extracted, then we can obtain:

$$l_s(G_i, G_j) = \frac{c(G_i) \cdot c(G_j) \cdot n}{\sum_{c \rightarrow n} c}, \quad (8)$$

$$l_d(G_i, G_j) = \frac{c(G_i) \cdot c(G_j) \cdot n}{\sum_{c \rightarrow n} c}, \quad (9)$$

where the numerator of l_s denotes the number of images sharing the common textual attributes with the images where the i -th and j -th graphlets are extracted; the numerator of l_d is the number of images having different textual attributes with the images where the i -th and j -th graphlets are extracted. The denominator represents the total number of images with all textual attributes, which functions as a normalization factor. Objective function (7) can be reorganized into:

$$\operatorname{argmin}_Y \sum_{ij} \|y_i - y_j\|^2 [l_s(i, j) - l_d(i, j)] = \operatorname{argmax}_Y \operatorname{tr}(YUY^T), \quad s.t. \quad YY^T = I \quad (10)$$

where $U = [-\vec{e}_{N-1}^T, \mathbf{I}_{N-1}]^T \mathbf{W}_1 [-\vec{e}_{N-1}^T, \mathbf{I}_{N-1}] + \dots + [-\vec{e}_{N-1}^T, \mathbf{I}_{N-1}]^T \mathbf{W}_t [-\vec{e}_{N-1}^T, \mathbf{I}_{N-1}]$ is an N^e , and $\times N$ diagonal matrix whose h -th diagonal element is $l_s(h, i) - l_d(h, i)$. Note that (10) is a quadratic problem with quadratic constraints, which can be solved by eigenvalue decomposition with a time complexity of $O(N^3)$. To accelerate the solution, an iterative coordinate propagation [31]-based embedding is applied.

Based on the manifold embedding algorithm, we calculate the attribute-level response map for each image. In particular, given D the number of textual attributes, we train a multiclass SVM based on the one-versus-rest scenario. The saliency response of graphlet G to textual attribute u_d is calculated based on the probabilistic output of SVM:

$$p(y(G) \rightarrow u_d) = \frac{1}{1 + \exp(-\phi_{u_d}(y(G)))}, \quad (11)$$

where $y(G)$ is the post-embedding vector corresponding to graphlet G , and $\phi_{u_d}(\cdot)$ denotes the classification hyper-plane separating graphlets belonging to images with textual attribute u_d from the rest of graphlets.

After obtaining the saliency map to each textual attribute, we randomly generate 10000 patches in each image. The patch sizes are tuned as follows: the patch width is tuned from $[0.1w, 0.9w]$ with a step of $0.01w$, while the patch height is tuned from $[0.1h, 0.9h]$ with a step of $0.01h$. Note that w and h denote the width and height of an image respectively. Then, the patch W whose internal graphlets' joint probability can be maximized is selected, *i.e.*,

$$\max_{G \square W} \prod p(y(G) \rightarrow u_d). \quad (12)$$

Patch W indicates the visual attribute that is most responsive to textual attribute u_d . It captures the aesthetically relevant visual feature and we therefore call it aesthlet.

C. Aesthlet-normalized CNN for Aesthetic Modeling

We integrate aesthlets into a deep architecture which learns patch-normalized representations to model visual attributes. After localizing different aesthlets using a weakly supervised manner, we normalize and feed them into a CNN for extracting standard representations for visual attributes modeling. To this end, we leverage both the power of CNN to learn discriminative visual features and the advantage of aesthlets to enhance CNN learning by localizing highly aesthetic regions. Noticeably, although CNN has been successfully applied to a variety of multimedia tasks, they cannot generalize well when are trained using small-scale data. Our proposed aesthlets make the learning process requiring fewer training examples due to the increased training set size. This is because a Flickr image usually contains multiple aesthlets, each of which is treated as a single training example.

Starting from a large collection of aesthlet patches, we resize each of them into 64×64 . Then, we randomly jitter each patch and flip it horizontally/vertically with probability 0.5 to improve the generalization, thereby a CNN is trained to represent each aesthlet. The architecture of the proposed CNN is elaborated in Fig. 3. The network contains four layers, *i.e.*, convolution, max pooling, local response normalization and a fully-connected layer with 1024 hidden units. Afterward the network branches out one fully connected layer containing 128 units to describe each visual attribute. The last two layers are split to form tailored features for each visual attribute, *e.g.*, determining whether a Flickr image is “brightly-colored” or “well-structured” will require different visual features. Comparatively, the bottom layers are shared in order to: 1) reduce the number of parameters, and 2) take advantage of the common low-layer CNN structure. The parameters of our developed CNN are adjusted by cross-validation. Specifically, we first set the entire parameters, *i.e.*, the input patch size, the number of convolutions, and the strides exactly the same as

those in Krizhevsky *et al.* [24]’s work. Then, we tune one parameter while leaving the rest unchanged. We set the tuning parameter by maximizing the accuracy of aesthetic prediction on our compiled data set [35].

The entire CNN is trained based on the standard backpropagation [16] of the error, combined with a stochastic gradient descent as a loss function, *i.e.*, the sum of the logloss of each aesthlet from a training image. The architecture of each CNN layer is shown in Fig. 3 and the implementation details are provided in [16]. To effectively handle noise, we employ aesthlet patches with high detection accuracies (based on (12)) in the training stage. In our paper, we adopted a pretrained network (trained from an image set by combining three aesthetic images data set: CHUK [33], PNE [3], and AVA [2]) to increase the aesthetic prediction performance. We exactly following the training phase of the deep architecture in [60]. The neural network consists of five convolutional layers, each which are followed by max-pooling layers and three fullyconnected layers with a final 1000-way softmax.

As shown in Fig. 4, each aesthlet describes the aesthetics

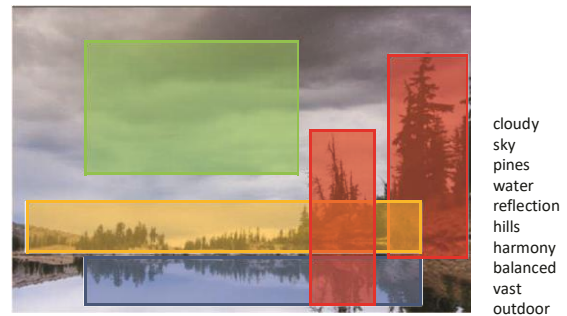


Fig. 4. Examples comparing the roles of global composition and aesthlets in describing image aesthetics. The color-tagged regions indicate aesthlets acquired using the Flickr tags on the right.

of a Flickr image in a single view. Therefore, we first utilize the developed CNN with respect to each aesthlet to generate representative aesthetic feature from a single view. Then, we combine the representations from multiple views to obtain the final aesthetic feature describing the entire image. More specifically, we extract the activations from the *fc attr* layer

in Fig. 3, which is 1024-dimensional, to describe each aesthlet. Finally, we concatenate the activations of all the aesthlets into a long feature vector. It is worth emphasizing that, if an aesthlet does not activate for an image, we set its corresponding feature representation to zero.

As exemplified in Fig. 4, the aforementioned aesthlet-based

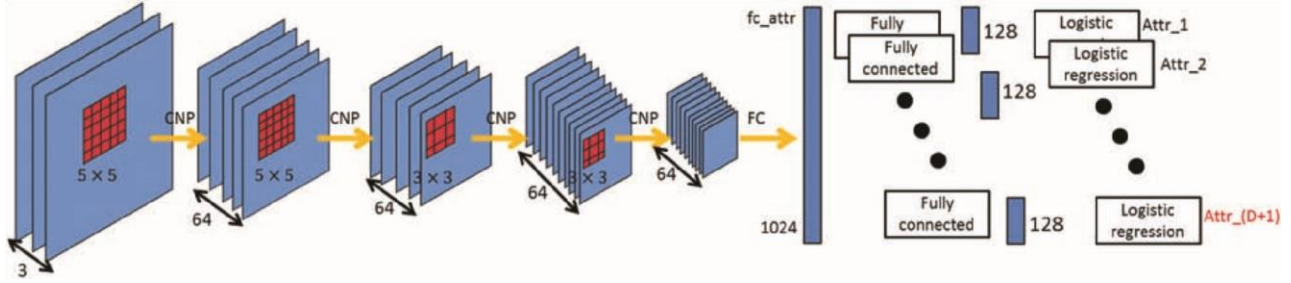


Fig. 3. A graphical illustration of the proposed deep architecture (CNP means convolution, normalization and pooling, and FC denotes the fully-connected layer. The $(D + 1)$ -th visual attribute corresponds to the aesthlet describing an entire Flickr image.)

CNN exploits regional visual features perceived by human beings. Nevertheless, global features also play an important role in describing image aesthetics. In general, however, aesthlet patches cannot cover the entire image region. Even worse, in some degenerated cases, a Flickr image may have very few detected aesthlets, *e.g.*, abstract paintings without specific objects. To deal with this, we also incorporate a CNN whose inputs are patches covering the whole Flickr image, in order to capture the global aesthetics of Flickr images. Obviously, patches covering the whole image can be considered as special aesthlets. Therefore, the CNN is implemented using the same structure as that shown in Fig. 3.

Lastly, we concatenate the feature vectors corresponding to all the aesthlets from each Flickr image into a $128 \times (D + 1)$ dimensional feature vector, which reflects the aesthetic feature of the image both locally and globally.

D. Applications of the Deep Aesthetic Features

We employ the learned deep aesthetic features to enhance three key applications in multimedia: photo retargeting, aesthetics-based image classification and retrieval.

Image retargeting: To demonstrate the descriptiveness

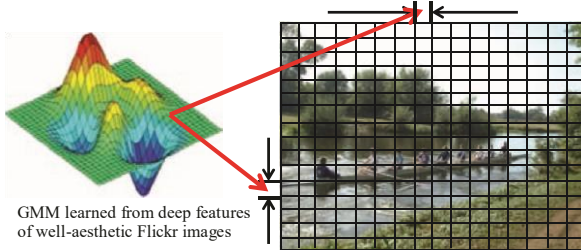


Fig. 5. Image retargeting based on the GMM learned from our deep features

of the deep aesthetic feature, we first apply it onto image retargeting. Specifically, we attempt to shrink a set of wide pictures (width/height=3/2) into a narrow one (width/height=2/3), where the aesthetically-pleasing elements can be optimally preserved. It is generally acknowledged that photo aesthetic assessment is a subjective task. Viewers with different backgrounds/experiences might have different opinions on the same picture. In order to reduce such bias, it is necessary to leverage the aesthetic experiences of multiple users. Herein, we learn the distribution of deep aesthetic features from a large collection of professional photographers.

For image retargeting, a 5-component GMM is deployed to

learn the distribution of deep features calculated from all the training aesthetically pleasing Flickr images:

$$p(z|\theta) = \sum_{l=1}^5 \alpha_l N(z|\pi_l, \Sigma_l), \quad (13)$$

where z denotes the deeply-learned features, and $\theta = \{\alpha_l, \pi_l, \Sigma_l\}$ are the GMM parameters.

Based on the GMM, we shrink a test image to make its deep feature most similar to those from the training images, as shown in Fig. 5. Particularly, we decompose an image into equal-sized grids. Afterward the horizontal (*w.r.t.* vertical) weight of grid ϕ is calculated as:

$$w_h(\phi) = \max p(z(\phi)|\theta), \quad (14)$$

where $z(\phi)$ denotes the deep aesthetic feature calculated by the shrunk image. After obtaining the horizontal (*w.r.t.* vertical) weight of each grid, a normalization step is carried out to make them sum to one:

$$\frac{w_h(\phi_i)}{\sum_i w_h(\phi_i)} = w_h^-(\phi_i), \quad (15)$$

Given the size of the retargeted image $W \times H$, the horizontal dimensionality of the i -th grid is shrunk to $\lceil W \cdot w_h^-(\phi_i) \rceil$, where $\lceil \cdot \rceil$ rounds a real number to the nearest integer. The shrinking operation along the vertical direction is similar to that along the horizontal direction.

Aesthetics-based image classification/retrieval: The objective of these two tasks is to show the ability of our designed deep feature in discriminating different aesthetic levels. Specifically, for aesthetics-based image classification, each picture is described by our designed deep aesthetic feature, and then we train a probabilistic model (as illustrated in Fig. 6) to identify whether a picture is highly or low aesthetic. For aesthetics-based image retrieval, for each query picture, we first calculate the aesthetic score of each picture from the database using the probabilistic model. Afterward, we output pictures in the database whose aesthetic scores are close to that of the query image.

The deep aesthetic feature reflects human aesthetic perception. They can be used to: 1) identify whether a Flickr image is highly or low aesthetic, and 2) aesthetics-based image retrieval. The key technique of these two applications is a probabilistic model.

As shown in Fig. 6, given a set of training images and a test one, they are highly correlated through their deep aesthetic features z and z^\square . The probabilistic model contains

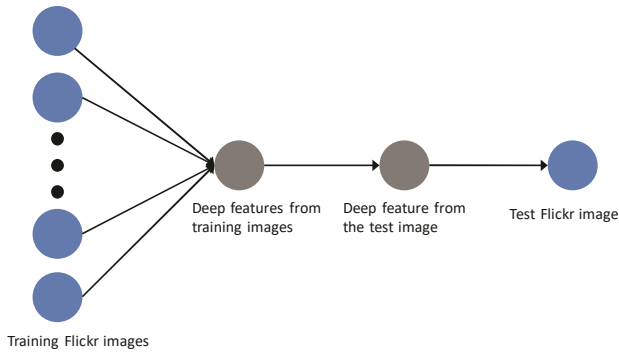


Fig. 6. A graphical illustration of the probabilistic model for image aesthetics quantification

four layers. The first layer corresponds to all the training images I^1, I^1, \dots, I^L which are aesthetically pleasing; the second layer denotes all the deep aesthetic features z learned from the training images; the third layer represents the deep aesthetic feature z^\square extracted from the test image; and the last layer denotes the test image I^\square .

Naturally, image aesthetics can be quantified as the amounts of deep aesthetic features that can be transferred from the training images into the test one. Therefore, the aesthetics of a test image can be quantified as:

$$\begin{aligned} \gamma &= p(I^\square | I^1, I^1, \dots, I^L) \\ &= p(I^\square | z^\square) \cdot p(z^\square | z) \cdot p(z | I^1, I^2, \dots, I^L), \quad (16) \end{aligned}$$

where the probability $p(z^\square | z)$ is calculated as: $p(z^\square | z) = \prod_{j=1}^L p(z_* | z^j)$. z_* is the deep aesthetic feature obtained from the test image. z^j denotes the deep aesthetic feature calculated from the j -th training image.

Following many algorithms [32], [35], we define the similarity between deep aesthetic features as a Gaussian kernel:

$$p(z^\square | z) \propto \exp\left(-\frac{\|z_* - z\|^2}{2\sigma^2}\right). \quad (17)$$

After obtaining the aesthetic score γ of a test Flickr image. If $\gamma > 0.5$, then this image is deemed as ‘‘aesthetically pleasing’’ and vice versa. Besides, for aesthetics-based image retrieval, we output images in the database whose aesthetic scores are similar to that of the query image.

IV. Experimental Results and Analysis

This section evaluates the performance of the proposed deep aesthetic feature based on four experiments. The first experiment visualizes and analyzes the effectiveness of the proposed aesthlet. Next, we compare the three applications based on our deeply-learned aesthetic feature with the state-of-

the-art. A step-by-step evaluation of the proposed method is presented subsequently. The last experiment evaluates the influence of different parameter settings.

All the experiments were carried out on a personal computer equipped with an Intel i5-2520M CPU and 8GB RAM. The algorithm was implemented on the Matlab 2012 platform.

A. Descriptiveness of the Proposed Aesthlet

As the input to our deep architecture, aesthlets are image patches which are aesthetically pleasing and correspond to the textual attributes in each Flickr image. In this experiment, we first visualize the extracted aesthlets on a subset of our collected Flickr image [34] dataset. Then, a comprehensive user study based on 132 participants is conducted to evaluate the descriptiveness of our proposed aesthlets.

Dataset Compilation: We spent significant time, effort, and resources to crawl photos from 35 well-known Flickr groups. For each group, we collected 70,000 \square 90,000 photos from nearly 7,400 Flickr users. The statistics of our dataset is shown in Fig. 7. For different Flickr groups, the numbers of photos belonging to each user varies from 10 to 220. We rank the Flickr images from each group based on the aesthetic measure by Zhang *et al.* [35]. The top 10% highly aesthetic photos constitute the image set.

We set the number of textual attributes D to 10 and

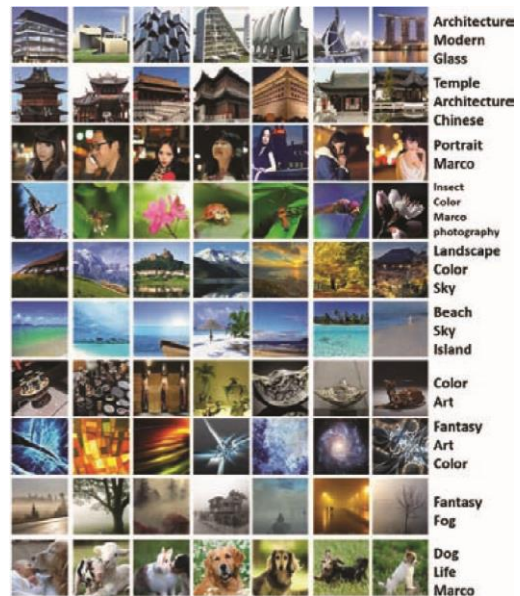


Fig. 8. Visualized aesthlets corresponding to each textual attribute

calculate the corresponding aesthlets according to (12). The representative aesthlets describing each textual attribute is presented in Fig. 8, and the following observations can be made:

- The learned textual attributes are representative to each Flickr image, as the corresponding visual attributes can accurately detect aesthetically pleasing regions in each image. Moreover, we notice that each Flickr image is associated with fewer than three textual attributes. This is achieved by the sparse LSA which can accelerate aesthetic modeling remarkably.

- Our graphlet-based weakly supervised learning algorithm effectively maps the textual attributes to the corresponding aesthlets. This is because graphlets can seamlessly capture objects with various shapes, and the weakly supervised algorithm can be solved analytically and efficiently.

(ISC) [37], optimized scale-and-sketch (OSS) [39] and saliencybased mesh parametrization (SMP) [40], and the patch-based wrapping (PW) [41]. Resolution of the output images is fixed to 640 (width) by 960 (height). The experimental images are all from the RetargetMe dataset [42]

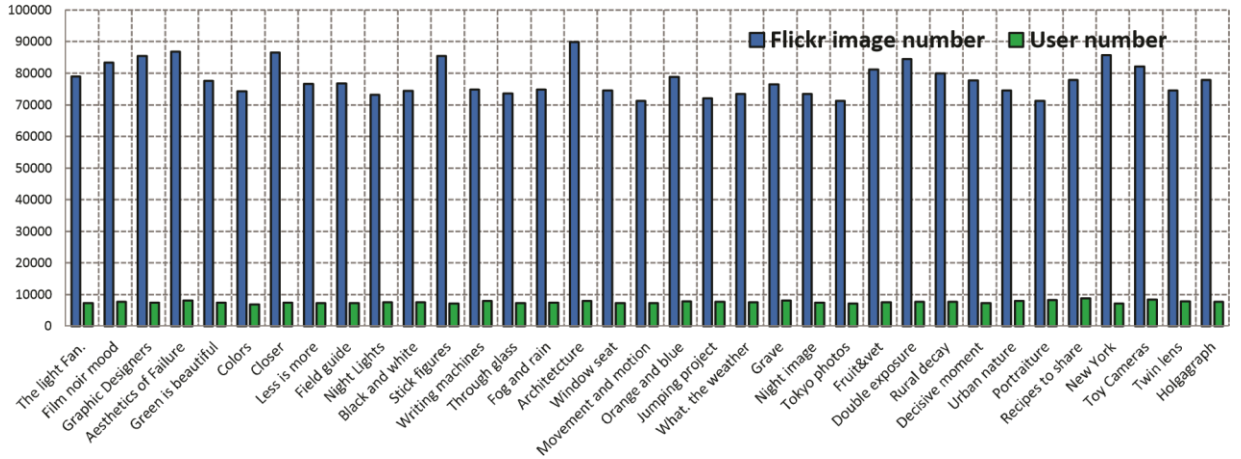


Fig. 7. The 35 Flickr groups (the horizontal axis) and the number of users (the vertical axis) in each group

- We notice that aesthlets corresponding to the same textual attribute have highly similar semantics, such as “modern architecture”. Simultaneously, aesthlets corresponding to different textual attributes have distinguishable semantics, such as “scenery” and “beach”. This demonstrates the effectiveness of our aesthlets discovering mechanism, since the ratio between inter-attribute scatter and intraattribute scatter is prone to be maximized.

As aesthlets reflect human aesthetic perception, it is infeasible to measure their descriptiveness quantitatively. In this experiment, we conduct a user study to evaluate them qualitatively. This strategy was also adopted in [35] for comparing the aesthetic quality of cropped photos. We invited 132 participants and most of them are master/Phd students from computer sciences department. For each aesthlet, we asked each participant to indicate its preference and discrimination scores. The former reflects the attractiveness of the aesthlet, while the latter shows whether the aesthlet captures a unique style of aesthetics. We set the number of textual attributes D to 10, 20, 40, 80 and 160 respectively. Then, the average preference and discrimination scores of aesthlets are calculated and reported in Table I. As can be seen, the preference scores under different values of D are above 0.9, which shows that the extracted aesthlets can accurately localize visually attractive regions. In contrast, the discrimination of aesthlet decreases dramatically when the value of D increases. The reason might be that the number of latent aesthetic types is much smaller than the number of textual attributes D .

B. Comparative Study

This subsection evaluates the three applications based on our deeply-learned aesthetic features: image retargeting, aesthetics-based image classification and retrieval.

Image retargeting: Fig. 9 compares the proposed method (PM) against several representative state-of-the-art approaches, including seam carving (SC) [38] and its improved version

In order to make the evaluation comprehensive, we adopt a paired comparison-based user study to evaluate the effectiveness of our proposed retargeting algorithm. In the paired comparison, each participant is presented with a pair of retargeted photos from two different approaches, and is required to indicate a preference as of which one they would choose for an iPhone wallpaper. In the user study, the participants are 40 amateur/professional photographers. As shown in Fig. 9, compared with its counterparts, our approach well preserves the semantically important objects in the original photos, such as the warship and the bubble car. In contrast, the compared retargeting methods sometimes shrink the semantically important objects, such as the viewer, the boy and the football player. Even worse, SC and its variant ISC, as well as OSS sometimes result in visual distortions.

In addition, we present an in-depth study of the user study on the 12 sets of retargeted photos displayed in Fig. 9, which is inspired by the comparative study of retargeting algorithms in [42]. Herein, μ denotes the average number of user scores, since the user study is carried out on a set of users. With reference means that we present each viewer with the original image and then ask him/her to score the lines/edges quality (*i.e.*, whether the lines or edges are nicely preserved in the retargeted image). As shown in Fig. 9, the average scores with original images are higher than those without original images. This is because, sometimes the original images are slightly distorted, and presenting the reference images can thus lead to a more fair evaluation. Meanwhile, without the original images, the scores are decided by how perfect the retargeted photos are. In this way, the scores are usually lower than those with reference images. We invited 132 volunteers and most of them are Master/Phd students from computer sciences department. For each volunteer, we asked them two questions: 1) Whether each visualized aesthlet is preferred by him/her and further indicate its aesthetic level, which is a real number ranging from 0 to 1. 0 indicates the lowest aesthetics while 1 denotes the highest aesthetics. 2) Whether each visualized aesthlet corresponding

TABLE I

Average preference and discrimination scores of aesthlets by varying D

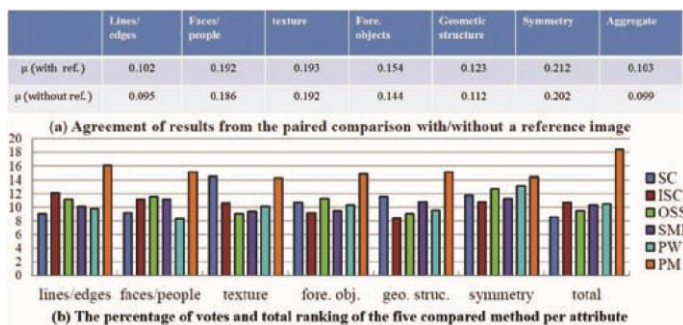
	$D=5$	$D=10$	$D=20$	$D=40$	$D=80$	$D=160$
Discrimination	0.9004	0.9432	0.8956	0.8211	0.7676	0.6545



to each textual attribute is distinguishable from those corresponding to the

Fig. 9. Photos retargeted based on different algorithms

rest textural attribute, and further quantify its discriminative level. 0 indicates the lowest discrimination while 1 denotes the highest discrimination. After collecting the preference and discrimination scores of all the aesthlets, we average them. Obviously, these two measures can show the effectiveness of our proposed method. First, we evaluate the degree of agreement when the volunteers vote for their favorite retargeted images, where a high disagreement reflects the difficulty in decision making. In our experiment, we use the coefficient of agreement defined by Kendall and Babington-Smith [62]. The coefficients over all the 12 retargeted images are shown in the last column of Fig. 10(a). Besides, we also collect the volunteers' votes on each attribute of the four sets of retargeted photos. As shown from the second column to the seventh



column in Fig. 10(a), the volunteers are highly agreeable on the face/people, the texture, and the symmetry because these attributes are well preserved by our retargeting model. Then, we present the votes on each attribute based on the 12 retargeted images. As shown in Fig. 10(b), the proposed method receives the most votes on all the attributes consistently.

Aesthetics-based image classification: We compare our approach with five image aesthetics evaluation methods. The compared methods include three global feature-based approaches proposed by Dhar *et al.* [5], Luo *et al.* [6], and Marchesotti *et al.* [7] respectively, as well as two local patch integration-based methods proposed by Cheng *et al.* [36]

Fig. 10. A detailed analysis of the comparative retargeted photos in Fig. 9

and Nishiyama *et al.* [10] respectively, and the CNN-based aesthetic model developed by Lu *et al.*. In [22], Lu *et al.* proposed a novel framework to predict image style, aesthetics, and quality. The key technique is a deep network which learns the fine-grained details from multiple image patches, where multi-patch aggregation functions are learned as part of the neural network training. Our proposed aesthlet-based image aesthetic model is significantly different from Lu *et al.*'s method, which is conducted in an unsupervised way. In our

approach, the image patches (*i.e.*, aesthlets) are detected by weakly-supervised learning, wherein the weak labels are latent topics detected from the M -dimensional augmented frequency

TABLE II

Comparative aesthetic quality prediction accuracies

	CUHK	PNE	AVA
Dhar <i>et al.</i>	0.7386	0.6754	0.6435
Luo <i>et al.</i>	0.8004	0.7213	0.6879
Marchesotti <i>et al.</i> (FV-Color-SP)	0.8767	0.8114	0.7891
Cheng <i>et al.</i>	0.8432	0.7754	0.8121
Nishiyama <i>et al.</i>	0.7745	0.7341	0.7659
Lu <i>et al.</i>	0.8043	0.8224	0.8213
The proposed method	0.8879	0.8622	0.8465

vector.

In the comparative study, we observe that the source codes of the five baseline methods are unavailable and some experimental details are not provided. This makes it difficult to implement them exactly. In our implementation, we try to enhance some components of the baseline methods. The following settings are employed. For Dhar’s approach, we use the public codes from Li *et al.* [44] to extract the attributes from each photo. These attributes are combined with the lowlevel features proposed by Yeh *et al.* [51] to train the aesthetic classifier. For Luo *et al.*’s approach, not only the low-level and high-level features in their publications are implemented, but also the six global features from Getlter *et al.* [52]’s paper are utilized to strengthen the aesthetic prediction ability. For Marchesotti *et al.*’s approach, similar to the implementation of Luo *et al.*’s method, the six additional features are also adopted. For Cheng *et al.*’s algorithm, we implement it as a simplified version of our method, where only 2-sized graphlets are utilized for aesthetics measure. It is worth emphasizing that, for the probabilistic aesthetics evaluation models proposed by Cheng *et al.*, Nishiyama *et al.* method, and us, if the aesthetic score is higher than 0.5, then this image is categorized as highly aesthetic, and vice versa.

We present the aesthetics prediction accuracies on the CUHK, PNE and AVA in Table II. The image tags (*e.g.*, “portraits”, “landscape”, and “clouds”) from the three datasets are assigned by ourselves. We hired 50 master/Phd students from our department to conduct the label annotation task. Each student spent 2 – 4 hours to annotate 500 – 700 images. All the images from the three data sets: the CHUK (12,000 images), the PNE (nearly 1700 images), and the AVA (about 25,000 images) are annotated. As shown, our approach outperforms Marchesotti *et al.*’s approach by nearly 2%, and exceeds the rest of the compared methods by over 6%. The results demonstrate the superiority of our method.

Aesthetics-guided image retrieval: We adopt the precision rate [54] to evaluate the performance of image retrieval based on our deeply-learned aesthetic features. Precision denotes the ratio of the number of relevant images (to the user) to the scope S , which is specified by the number of top-ranked images. In the experiment, we observe that it is sufficient to display 30 retrieved images on a screen. Presenting more images may decrease their quality. Therefore, we set $S = 30$ throughout the experiment. The experimental dataset is our crawled largescale Flickr images from 35 groups.

In the current image retrieval systems, typically the query image is not existed in the image database. To handle this, we randomly select 30 images from each Flickr group as the query ones, while the rest are treated as the database for retrieval. Notably, the precision rate is calculated by averaging the results over the 30 – 35 = 1050 queries.

To alleviate computational burden, we select the most informative images from the top 400 images. Relevance feedback is employed to bridge the semantic gap in the retrieval system. The relevance feedback system contains the following stages:

i) users are shown 30 images which are considered as the most informative by SVM_{active} , where SVM_{active} denotes the active learning with support vector machine [53]; ii) users give relevance feedback; iii) (i) is repeated taking into account feedback from ii). Users are asked to make relevance judgements toward the queries results. Thereafter, the feedback information is utilized to re-rank the images in the database. SVM_{active} is utilized as the relevance feedback algorithm. It provides users with the most informative images with respect to the ranking function.

We compare our deep features with popular aesthetic descriptors proposed by Marchesotti *et al.* [7], Cheng *et al.* [36], Lu *et al.* [22], and Champbell *et al.* [23] respectively. As shown in Table III, in most of the 35 Flickr groups, our deeply-learned aesthetic feature achieves the highest precision. We also observe that, although Marchesotti *et al.*’s aesthetic feature is simple, its performance is competitive.

C. Step-by-step Model Justification

This experiment validates the effectiveness of the three key components in our deep aesthetic feature learning pipeline: 1) sparsity-constrained textual attributes discovery; 2) weakly supervised visual attributes localization; and 3) the aesthetnormalized CNN training. To empirically demonstrate the effectiveness and inseparability of these components, we replace each component by a functionally reduced counterpart and report the corresponding performance. We focus on the application of aesthetics-based image classification.

Step 1: To demonstrate the usefulness of the sparse textual discovery, three experimental settings are utilized to weaken the adopted sparse LSA. First, we abandon the sparsity constraint in (4). Afterward, we replace the sparse LSA by the well-known popular discriminate analysis (LDA) and principle component analysis (PCA) respectively. We present the calculated image classification accuracies in Table IV. As can be seen, removing the sparsity constraint results in an accuracy decrement of 5.2% on average. Moreover, neither LDA nor PCA can optimally discover the latent textual attributes, since their performances lag behind ours by over 10 %.

Step 2: To evaluate the effectiveness of the weakly supervised visual attributes learning, three experimental settings are adopted. We first replace the graphlet-based object detection by the objectness measure [56] and the part-based object detector [57] respectively. Then, we replace the superpixelbased spatial pyramid by the standard grid-based one. As shown in Table IV, on average, both the objectness and part-based detector cause a nearly 1.2% accuracy decrement. Notably, the training process of them requires manually annotated windows, which might be computationally intractable.

TABLE III

Precision at top 30 returns of the five compared aesthetic features. The highest precision is in bold for each Flickr group.

Flickr group	March.	ChengLu	Champ.	Ours	
The light Fan.	0.34	0.33	0.43	0.31	0.53
Film noir Mood	0.16	0.19	0.23	0.16	0.26
Graphic designers	0.33	0.27	0.31	0.24	0.29
Aesthetics failure	0.11	0.09	0.15	0.12	0.19
Green is beautiful	0.14	0.13	0.16	0.12	0.22
Colors	0.34	0.25	0.28	0.21	0.31
Closer	0.43	0.41	0.45	0.36	0.51
Less is more	0.26	0.22	0.25	0.21	0.34
Field guide	0.34	0.31	0.33	0.28	0.41
Night lights	0.16	0.14	0.16	0.13	0.19
Black and white	0.21	0.18	0.19	0.15	0.18
Stick figure	0.43	0.41	0.34	0.37	0.47
Writing mach.	0.67	0.64	0.68	0.56	0.76
Through glass	0.09	0.09	0.07	0.05	0.12
Fog and rain	0.21	0.20	0.18	0.19	0.25
Architecture	0.54	0.53	0.54	0.46	0.59
Window seat	0.42	0.39	0.40	0.36	0.46
Movement	0.35	0.31	0.33	0.31	0.37
Orange and blue	0.18	0.16	0.18	0.13	0.21
Jump Project	0.26	0.24	0.19	0.22	0.31
What. the weather	0.14	0.12	0.11	0.10	0.17
Grave	0.28	0.24	0.26	0.21	0.31
Night images	0.14	0.16	0.12	0.11	0.19
Tokyo photos	0.24	0.21	0.19	0.19	0.26
Fruit&vet	0.65	0.62	0.61	0.62	0.69
Double exposure	0.28	0.23	0.24	0.19	0.32
Rural decay	0.25	0.23	0.24	0.19	0.28
Decisive moment	0.24	0.22	0.19	0.17	0.27
Urban nature	0.32	0.26	0.27	0.23	0.29
Portraiture	0.54	0.46	0.48	0.47	0.59
Recipes to share	0.26	0.22	0.24	0.21	0.31
New York	0.27	0.23	0.25	0.21	0.31
Toy cameras	0.37	0.31	0.31	0.30	0.42
Twin lens	0.26	0.22	0.24	0.21	0.29
Holgagraph	0.33	0.28	0.25	0.21	0.38
Average	0.28	0.23	0.21	0.19	0.33

Besides, grid-based spatial pyramid severely decreases the performance of aesthetics-based image classification. The reason is that, compared with the superpixel-based graphlets, gridbased graphlets cannot well fit the complicated object shapes. Step 3: We study the performance of our developed CNN. We abandon the fully-connected layer and observe that the aesthetics-based classification reduces by 4% on average. This result reflects the necessity to explore the common low-layer CNN structure. Additionally, we abandon the global image visual attribute. On average, a decrement of nearly 7% is observed. This shows the importance of explicitly modeling global image configurations in aesthetic modeling.

D. Parameter Analysis

In this experiment, we evaluate the influence of important parameters in our proposed aesthetic model: 1) the number of textual attributes D , 2) the regularizer weight λ in sparse LSA, and 3) the structure of our designed CNN.

First, we tune D from five to 80 with a step of five and report the performance of aesthetics-based image classification. As shown in Fig. 11, on all the three datasets, the best accuracies

are achieved when D is 10 or 15. This indicates that there are about 10 \square 15 latent semantic categories from

TABLE IV
Performance decrement by varying the experimental settings in each component

	CUHK	PNE	AVA
Step 1: Sparsity	5.4%	4.9%	5.2 %
Step 1: Remove LSA	7.5%	6.7%	7.1 %
Step 1: LDA	9.6%	10.9%	10.3 %
Step 1: PCA	11.3%	9.5%	10.7 %
Step 2: Objectness	1.3%	1.0%	1.1 %
Step 2: Part-based	1.1%	1.1%	1.4 %
Step 2: Superpixel	7.9%	8.4%	7.3 %
Step 3: Fully-connected	4.3%	3.8%	4.0 %
Step 3: Remove global descriptor	8.4%	6.2%	6.7 %
Step 3: Only global descriptor	12.3%	14.1%	12.7 %

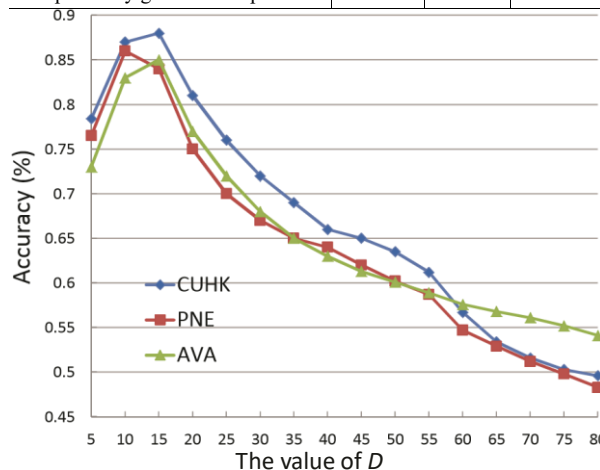


Fig. 11. Aesthetics-based image classification accuracies by varying D on the CUHK, PNE and AVA datasets

each of the three datasets. Second, we choose the value of λ from $\{0.5, 0.2, 0.1, 0.05, 0.001\}$ and report the corresponding accuracies. As shown in Table V, we notice that the best accuracies on all the three datasets are achieved when $\lambda = 0.1$. Next, we testify the effectiveness of our developed five-layered CNN. We change our CNN to a four- and six-layered CNN respectively. It is noticeable that the aesthetics-based image classification accuracies are decreased by 4.3% and 6.7 % respectively. Actually, in our implementation, the five CNN layers are validated by cross validations. Lastly, we preserve only the global descriptor for image aesthetics prediction, where the CNN-based descriptor is removed. As shown in the last row of Table V, aesthetics-based image classification using only global descriptor results in an accuracy decrement of 13% on average. This observation clearly demonstrates the necessity of leveraging local descriptors in aesthetic modeling.

TABLE V
Aesthetics-based image classification accuracies under different values of λ

Dataset	$\lambda = 0.5$	$\lambda = 0.2$	$\lambda = 0.1$	$\lambda = 0.05$	$\lambda = 0.001$
---------	-----------------	-----------------	-----------------	------------------	-------------------

CHUK	0.7612	0.8133	0.8879	0.6454	0.7687
PNE	0.7453	0.8231	0.8622	0.7121	0.7453
AVA	0.8113	0.8214	0.8465	0.7376	0.7786

V. Conclusions and Future Work

Perceptually aesthetic model is an important topic in multimedia [47], [48], [49], [50], [61], [62], [63] and computer vision [58], [59], [45], [46]. This paper proposes a CNN framework to hierarchically model how humans perceive aesthetically pleasing regions in each Flickr image. We first calculate a compact set of textual attributes from those tagged Flickr images using a sparsity-constrained LSA. Then, a weakly supervised learning algorithm projects the textual attributes onto the corresponding aesthlets in each image. These aesthlets capture visually attractive image regions and are deployed to train a CNN which mimicks human aesthetic perception. Based on the CNN, we represent each Flickr image by a set of deeply-learned aesthetic features, which can enhance a series of media applications, e.g., image retargeting, aesthetics-based image classification and retrieval.

In the future, this work will be extended to a more comprehensive deep architecture that encodes auxiliary visual cues such as exposure, contrast and symmetry.

References

- [1] Thomas Hofmann, Probabilistic Latent Semantic Analysis, in *Proc. of UAI*, 1999.
- [2] Luca Marchesotti, Naila Murray, Florent Perronnin, Discovering Beautiful Attributes for Aesthetic Image Analysis, *IJCV*, 10.1007/s11263-0140789-2, 2014.
- [3] Ritendra Datta, Dhiraj Joshi, Jia Li, James Z. Wang, Studying Aesthetics in Photographic Images using a Computational Approach, in *Proc. of ECCV*, 2006.
- [4] Yan Ke, Xiaoou Tang, Feng Jing, The Design of High-level Features for Photo Quality Assessment, in *Proc. of CVPR*, 2006.
- [5] Sagnik Dhar, Vicente Ordonez, Tamara L. Berg, High Level Describable Attributes for Predicting Aesthetics and Interestingness, in *Proc. of CVPR*, 2011.
- [6] Wei Luo, Xiaogang Wang, Xiaoou Tang, Content-based Photo Quality Assessment, in *Proc. of ICCV*, 2011.
- [7] Luca Marchesotti, Florent Perronnin, Diane Larlus, Gabriela Csurka, Assessing the Aesthetic Quality of Photographs using Generic Image Descriptors, in *Proc. of ICCV*, 2011.
- [8] Bin Cheng, Bingbing Ni, Shuicheng Yan, Qi Tian, Learning to Photograph, *ACM MM*, 2010.
- [9] Masashi Nishiyama, Takahiro Okabe, Yoichi Sato, Imari Sato, Sensation-based Photo Cropping, *ACM MM*, 2009.
- [10] Masashi Nishiyama, Takahiro Okabe, Imari Sato, Yoichi Sato, Aesthetic Quality Classification of Photographs based on Color Harmony, in *Proc. of CVPR*, 2011.
- [11] Subhabrata Bhattacharya, Rahul Sukthankar, Mubarak Shah, A Framework for Photo-Quality Assessment and Enhancement based on Visual Aesthetics, *ACM MM*, 2010.
- [12] Luming Zhang, Yue Gao, Roger Zimmermann, Qi Tian, Xuelong Li, Fusion of Multi-Channel Local and Global Structural Cues for Photo Aesthetics Evaluation, *IEEE T-IP*, 23(3): 1419–1429, 2014.
- [13] Luming Zhang, Yue Gao, Rongrong Ji, Qionghai Dai, Xuelong Li, Actively Learning Human Gaze Shifting Paths for Photo Cropping, *IEEE T-IP*, 23(5): 2235C2245, 2014.
- [14] Ali Sharif Razavian, Hossein Azizpour, Josephine Sullivan, Stefan Carlsson, CNN Features off-the-shelf: an Astounding Baseline for Recognition, *arXiv preprint arXiv:1403.6382*, 2014.
- [15] Jeff Donahue, Yangqing Jia, Oriol Vinyals, Judy Hoffman, Ning Zhang, Eric Tzeng, Trevor Darrell, DeCAF: A Deep Convolutional Activation Feature for Generic Visual Recognition, in *Proc. of ICML*, 2014.
- [16] Alex Krizhevsky, Ilya Sutskever, Geoffrey E. Hinton, ImageNet Classification with Deep Convolutional Neural Networks, in *Proc. of NIPS*, 2012.
- [17] Ning Zhang, Manohar Paluri, MarcAurelio Ranzato, Trevor Darrell, Lubomir Bourdev, PANDA: Pose Aligned Networks for Deep Attribute Modeling, in *Proc. of CVPR*, 2014.
- [18] Ping Luo, Xiaogang Wang, Xiaoou Tang, A Deep Sum-Product Architecture for Robust Facial Attributes Analysis, in *Proc. of ICCV*, 2013.
- [19] Ning Zhang, Jeff Donahue, Ross Girshick, Trevor Darrell, Part-based R-CNNs for Fine-grained Category Detection, in *Proc. of ECCV*, 2014.
- [20] Pierre Sermanet, Koray Kavukcuoglu, Soumith Chintala, Pedestrian Detection with Unsupervised Multi-Stage Feature Learning, in *Proc. of CVPR*, 2014.
- [21] Lin Sun, Kui Jiay, Tsung-Han Chany, Yuqiang Fang, Gang Wang, Shuicheng Yan, DL-SFA: Deeply-Learned Slow Feature Analysis for Action Recognition, in *Proc. of CVPR*, 2014.
- [22] Xin Lu, Zhe Lin, Hailin Jin, Jianchao Yang, James Z. Wang, RAPID: Rating Pictorial Aesthetics using Deep Learning, *ACM MM*, 2014.
- [23] Allan Campbell, Vic Ciesielksi, A. K. Qin, Feature Discovery by Deep Learning for Aesthetic Analysis of Evolved Abstract Images, *Evolutionary and Biologically Inspired Music, Sound, Art and Design Lecture Notes in Computer Science*, 9027: 27–38, 2015.
- [24] Jia Deng, Wei Dong, Richard Socher, Li-Jia Li, Kai Li, Li Fei-Fei, ImageNet: A Large-Scale Hierarchical Image Database, in *Proc. of CVPR*, 2009.
- [25] Scott Deerwester, Susan T. Dumais, George W. Furnas, Thomas K. Landauer, Richard Harshman, Indexing by Latent Semantic Analysis, *Journal of American Society for Information Sciences*, 41(6): 391–407, 1990.
- [26] Xi Chen, Yanjun Qi, Bing Hai, Qihang Lin, Jaime G. Garbonell, Sparse Latent Semantic Analysis, in *Proc. of NIPS*, 2010.
- [27] Robert Tibshirani, Regression Shrinkage and Selection via the Lasso, *Journal of the Royal Statistical Society: Series B*, 58: 267–288, 1996.
- [28] Jerome Friedman, Trevor Hastie, Rob Tibshirani, Regularization Paths for Generalized Linear Models via Coordinate Descent, *Journal of Statistical Software*, 33(1): 2010.
- [29] Markus Stricker, Markus Orengo, Similarity of Color Images, *Storage and Retrieval of Image and Video Databases*, 1995.
- [30] Navneet Dalal, Bill Triggs, Histograms of Oriented Gradients for Human Detection, in *Proc. of CVPR*, 2005.
- [31] Shiming Xiang, Feiping Nie, Yangqiu Song, Changshui Zhang, Chunxia Zhang, Embedding New Data Points for Manifold Learning via Coordinate Propagation, *Knowledge and Information Systems*, 19(2): 159C184, 2008.
- [32] Mingli Song, Dacheng Tao, Chun Chen, Jiajun Bu, Jiebo Luo, Chengqi Zhang, Probabilistic Exposure Fusion, *IEEE T-IP*, 21(1): 341–357, 2012.
- [33] Yan Ke, Xiaoou Tang, Feng Jing, The Design of High-level Features for Photo Quality Assessment, in *Proc. of CVPR*, 2006.
- [34] Luming Zhang, Roger Zimmermann, Flickr Circles: Mining Socially-Aware Aesthetic Tendency, in *Proc. of ICME*, 2015.
- [35] Luming Zhang, Mingli Song, Qi Zhao, Xiao Liu, Jiajun Bu, Chun Chen, Probabilistic Graphlet Transfer for Photo Cropping, *IEEE T-IP*, 21(5): 2887–2897, 2013.
- [36] Bin Cheng, Bingbing Ni, Shuicheng Yan, Qi Tian, Learning to Photograph, *ACM MM*, 2010.
- [37] Michael Rubinstein, Ariel Shamir, Shai Avidan, Improved Seam Carving for Video Retargeting, *ACM TOG*, 27(3), 16, 2008.
- [38] Shai Avidan, Ariel Shamir, Seam Carving for Content-Aware Image Resizing, *ACM TOG*, 26(3), 2007.
- [39] Yu-Shuen Wang, Chiew-Lan Tai, Olga Sorkine, Tong-Yee Lee, Optimized Scale-and-Stretch for Image Resizing, *ACM TOG*, 27(5), 118, 2008.
- [40] Yanwen Guo, Feng Liu, Jian Shi, Zhihua Zhou, Michael Gleicher, Image Retargeting Using Mesh Parameterization, *IEEE T-MM*, 11(5): 856–867, 2009.
- [41] Shih-Syun Lin, I-Cheng Yeh, Chao-Hung Lin, Tong-Yee Lee, PatchBased Image Warping for Content-Aware Retargeting, *IEEE T-MM*, 15(2): 359–368, 2013.
- [42] Michael Rubinstein, Diego Gutierrez, Olga Sorkine, Ariel Shamir, A Comparative Study of Image Retargeting, *ACM TOG*, 29(5), 160, 2010.
- [43] Michael Rubinstein, Ariel Shamir, Shai Avidan, Multi-operator Media Retargeting, *ACM TOG*, 28(3), 23, 2009.

[44] Fei-Fei Li, Pietro Perona, A Bayesian Hierarchical Model for Learning Natural Scene Categories, *in Proc. of CVPR*, 2005.

[45] Guokang Zhu, Qi Wang, Yuan Yuan, Pingkun Yan, Learning Saliency by MRF and Differential Threshold, *IEEE Y-CYB*, 43(6), pages: 2032 – 2043, 2013.

[46] Dapeng Tao, Lianwen Jin, Zhao Yang, Xuelong Li, Rank Preserving Sparse Learning for Kinect Based Scene Classification, *IEEE T-CYB*, 43(5), pages: 1406–1417, 2013.

[47] Li Liu, Ling Shao, Xiantong Zhen, Xuelong Li, Learning Discriminative Key Poses for Action Recognition, *IEEE T-CYB*, 43(6), pages: 1860– 1870, 2013.

[48] Ling Shao, Xiantong Zhen, Dacheng Tao, Xuelong Li, Spatio-Temporal Laplacian Pyramid Coding for Action Recognition, *IEEE T-CYB*, 44(6), pages: 817–827, 2013.

[49] Hong Qiao, Peng Zhang, Bo Zhang, Suiwu Zheng, Learning an Intrinsic Variable Preserving Manifold for Dynamic Visual Tracking, *IEEE TSMC-C*, 40(3), pages: 868–880, 2010.

[50] Changyou Chen, Junping Zhang, Rudolf Fleischer, Distance Approximating Dimension Reduction of Riemannian Manifolds, *IEEE T-CYB*, 40(1), pages: 208–217, 2010.

[51] Che-Hua Yeh, Yuan-Chen Ho, Brian A. Barsky, Ming Ouhyoung, Personalized Photograph Ranking and Selection System, *ACM MM*, 2010.

[52] Peter Gehler, Sebastian Nowozin, On Feature Combination for Multiclass Object Classification, *in Proc. of ICCV*, 2009.

[53] Jan Kremer, Kim Steenstrup Pedersen, Christian Igel, Active Learning with Support Vector Machines, *in Proc. of NIPS*, 2014.

[54] Dionysius P. Huijsmans, Nicu Sebe, How to Complete Performance Graphs in Content-based Image Retrieval: Add Generality and Normalize Scope, *IEEE T-PAMI*, 27(2): 245–251, 2005.

[55] Victor Escorcia, Juan Carlos Niebles, Bernard Ghanem, On the Relationship between Visual Attributes and Convolutional Networks, *in Proc. of CVPR*, 2015.

[56] Bogdan Alexe, Thomas Deselaers, Vittorio Ferrari, Measuring the Objectness of Image Windows, *IEEE T-PAMI*, 34(11): 2189–2202, 2012.

[57] Pedro F. Felzenszwalb, Ross B. Girshick, David A. McAllester, Deva Ramanan, Object Detection with Discriminatively Trained Part-Based Models, *IEEE T-PAMI*, 32(9): 1627–1645, 2010.

[58] Guokang Zhu, Qi Wang, Yuan Yuan, NATAS: Neural Activity Trace Aware Saliency, *IEEE Y-CYB*, pages: 73–80, 2013.

[59] Qi Wang, Yuan Yuan, Pingkun Yan, Xuelong Li, Saliency Detection by Multiple-Instance Learning, *IEEE Y-CYB*, 43(2), pages: 660–672, 2013.

[60] Alex Krizhevsky, Ilya Sutskever, Geoffrey E. Hinton, ImageNet Classification with Deep Convolutional Neural Networks, *in Proc. of NIPS*, 2012.

[61] Luming Zhang, Yue Gao, Rongrong Ji, Lv Ke, Jiale Shen, Representative Discovery of Structure Cues for Weakly-Supervised Image Segmentation, *IEEE T-MM*, 16(2): 470–479, 2014

[62] Luming Zhang, Yue Gao, Chaoqun Hong, Yinfu Feng, Jianke Zhu, Deng Cai, Feature Correlation Hypergraph: Exploiting High-order Potentials for Multimodal Recognition, *IEEE T-CYB*, 44(8), pages: 1408–1419 , 2014.

[63] Luming Zhang, Mingli Song, Yi Yang, Qi Zhao, Chen Zhao, Nicu Sebe, Weakly Supervised Photo Cropping, *IEEE T-MM*, 16(1), pages: 94–107, 2014.

PLACE
PHOTO
HERE

PLACE
PHOTO
HERE

PLACE
PHOTO
HERE

PLACE
PHOTO
HERE

PLACE
PHOTO
HERE

Yanxiang Chen received the Ph.D. degree from Electronic Science and Technology in University of Science & Technology of China (USTC) in 2004 .As a visiting scholar, she has been to Beckman Institute at University of Illinois at Urbana- Champaign (UIUC) from August 2006 to April 2008, and Department of Electronic Computer Engineering at the National University of Singapore (NUS) from November 2012 to February 2013. She is

a SPIE member, ACM member, and CCF member. Her work has been supported by the Natural Science Foundation of China, Natural Science Foundation of Anhui Province of China, and Postdoctoral Science Foundation of China. Her current research fields include audio-visual signal processing, saliency and scene analysis.

Yuxing Hu received the B.Eng. degree in automatic engineering from Southeast University, Nanjing, China, in 2011, and is currently working towards the Ph.D. degree at Tsinghua University, Beijing, China. His main research interests include analog integrated circuit design, biomedical electronics, and figure processing.

Luming Zhang (M’14) received his Ph.D. student in computer science from Zhejiang University, China. Currently he is a faculty at Hefei University of Technology, China. His research interests include visual perception analysis, image enhancement, and pattern recognition.

Ping Li received the B.Eng. degree in automatic engineering from Southeast University, Nanjing, China, in 2011, and is currently working towards the Ph.D. degree at Tsinghua University, Beijing, China. His main research interests include analog integrated circuit design, biomedical electronics, and figure processing.

Chao Zhang is a Ph.D. student at the Computer Science Department, University of Illinois at UrbanaChampaign. Prior to joining UIUC, he earned his B.S. and M.S. degrees from Zhejiang University, China. His research interests include spatiotemporal data mining, social media analysis, and applied machine learning.